

Evaluation of Four-dimensional (4D) Computed Tomography (CT) Pulmonary Ventilation Imaging by Comparison with Single Photon Emission Computed Tomography (SPECT) Scans for a Lung Cancer Patient

Tokihiro Yamamoto¹, Sven Kabus², Jens von Berg², Cristian Lorenz², Michael L. Goris³, Billy W. Loo, Jr.¹ and Paul J. Keall¹

¹ Department of Radiation Oncology, Stanford University School of Medicine, Stanford, CA, USA

Tokihiro@stanford.edu

² Department of Digital Imaging, Philips Research Europe, Hamburg, Germany

³ Division of Nuclear Medicine, Stanford University School of Medicine, Stanford, CA, USA

Abstract. The goal of this study was to present a method for physiologic validation and show results for a comparison of the 4D-CT ventilation and SPECT ventilation or perfusion. A 4D-CT and a SPECT ventilation/perfusion (V/Q) (V_{SPECT} and Q_{SPECT}) scans were acquired for a lung cancer patient. Two 4D-CT ventilation images were created using two metrics: Hounsfield unit (HU)-change ($V_{4\text{D-CT}}^{\text{HU}}$) and Jacobian determinant ($V_{4\text{D-CT}}^{\text{Jac}}$), and were compared with SPECT. The 4D-CT ventilation images were of higher resolution than SPECT. Areas of visual agreement and disagreement were identified. V_{SPECT} suffered from central airway depositions. Quantitatively, the correlation coefficients with V_{SPECT} (Q_{SPECT}) were 0.030 (0.357) for $V_{4\text{D-CT}}^{\text{HU}}$, and 0.184 (0.479) for $V_{4\text{D-CT}}^{\text{Jac}}$. The physiologic accuracy of 4D-CT ventilation imaging has been evaluated on a human subject. The weak correlations with SPECT could be due to limitations of the 4D-CT and/or SPECT techniques. Further investigation and patient studies are needed.

Keywords: Lung, functional imaging, ventilation, four-dimensional (4D) computed tomography (CT), single photon emission CT (SPECT).

1 Introduction

Imaging techniques of regional pulmonary function would further our understanding of pathophysiological characteristics of pulmonary diseases and also could be used for functional avoidance in lung cancer radiotherapy. Regional pulmonary function can be represented by ventilation or perfusion. There are several techniques for ventilation imaging which includes nuclear medicine imaging (the current standard of care) [1], hyperpolarized gas magnetic resonance (MR) imaging [2], and Xe gas computed tomography (CT) imaging [3]. These techniques have drawbacks such as

low resolution, high cost, long scan time, and/or low accessibility. Ventilation images can be created by a novel four-dimensional (4D) CT-based technique in three steps, by (1) acquisition of 4D-CT scans, (2) spatial voxel-wise mapping of different respiratory phases of 4D-CT images using deformable image registration (DIR), and (3) quantitative analysis of the resultant displacement vector fields (DVs) for computing the ventilation metric. Guerrero et al. have originally developed this method using paired breath-hold CT images [4]. They used DIR to map the peak-exhale CT image to the peak-inhale image, and calculated the change in the fraction of air per voxel as regional ventilation based on the theory proposed by Simon [5]. Several investigators have applied this approach to 4D-CT images with some modifications [6-10]. The 4D-CT ventilation can be considered as ‘free’ information, because 4D-CT scans are in routine use for lung cancer radiotherapy in many centers, and ventilation computation involves only image processing (i.e., DIR) and analysis. Moreover, 4D-CT ventilation imaging has high resolution, low cost, short scan time, and high accessibility. There are various DIR algorithms and two ventilation metrics that have been and could be used for 4D-CT ventilation imaging [4, 6-10]. Variability in the DIR results between algorithms has been reported [11, 12], which could potentially impact 4D-CT ventilation imaging. To date there has been limited physiologic validation of 4D-CT ventilation imaging. Reinhardt et al. demonstrated a reasonably high correlation (average, $R^2 = 0.73$) between the average ventilation values in 4 mm thick sub-regions determined by the 4D-CT ventilation and Xe-CT for 5 anesthetized sheep [8]. Yamamoto et al. compared the 4D-CT ventilation in emphysematous (i.e., known low signal regions) and non-emphysematous lung regions for 12 patients, and demonstrated significantly lower ventilation in emphysema ($p < 0.001$) [13]. More recently, Castillo et al. compared the 4D-CT ventilation and single photon emission CT (SPECT) ventilation for seven patients, however demonstrated low Dice similarity coefficients (i.e., < 0.4 on average) for the functional lung segments. More thorough validation is clearly needed for human subjects. The goal of this study was to present a method for physiologic validation and show quantitative results for a comparison of the 4D-CT ventilation and SPECT ventilation or perfusion in a lung cancer patient.

2 Methods and Materials

First, we acquired a 4D-CT and a SPECT ventilation/perfusion (V/Q) (V_{SPECT} and Q_{SPECT}) scans for a lung cancer patient. Second, we created 4D-CT ventilation images. Two different 4D-CT ventilation images were created using two metrics: Hounsfield unit (HU)-change ($V_{4\text{D-CT}}^{\text{HU}}$) [4, 5, 7, 10, 13] and Jacobian determinant ($V_{4\text{D-CT}}^{\text{Jac}}$) [7, 8, 13]. Finally, we quantified the physiologic accuracy of 4D-CT ventilation imaging by comparison with V_{SPECT} and Q_{SPECT} . Here we define the physiologic accuracy as the voxel-based correlation between the 4D-CT ventilation and SPECT. Fig. 1 shows a schematic diagram for this process. $V_{4\text{D-CT}}^{\text{HU}}$ and $V_{4\text{D-CT}}^{\text{Jac}}$ were created in three steps, by (1) acquisition of 4D-CT scans, (2) spatial voxel-wise mapping of the peak-exhale 4D-CT image to the peak-inhale image using DIR,

and (3) quantitative analysis of the resultant DVFs for computing the ventilation metric (see the section 2.2 for more details). We also performed a SPECT/CT V/Q scan (see the section 2.3). Each of V and Q scans consisted of a low-dose CT acquisition followed by a SPECT acquisition. For the 4D-CT ventilation to SPECT comparison, the CT image of SPECT was aligned with the peak-exhale 4D-CT image using rigid image registration. The derived translations and rotations were applied to the SPECT images to align with the 4D-CT ventilation images, assuming that the patient did not move between the SPECT and CT scans.

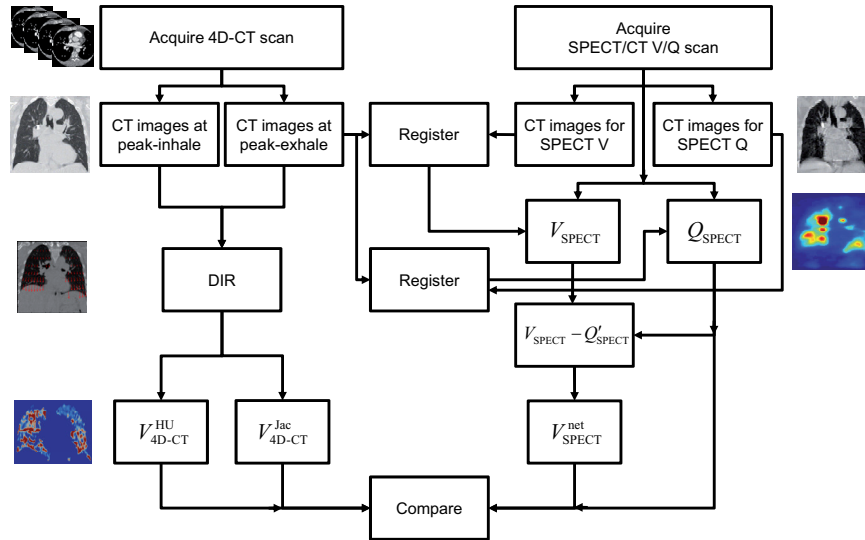


Fig. 1. A schematic diagram for creating 4D-CT ventilation images, acquiring SPECT/CT V/Q images, and comparing these images. For 4D-CT ventilation imaging, deformable image registration (DIR) was performed for spatial voxel-wise mapping of the peak-exhale 4D-CT image to the peak-inhale image. Resultant displacement vector fields were analyzed to create ventilation images using two different metrics: Hounsfield unit (HU)-change (V_{4D-CT}^{HU}) and Jacobian determinant of deformation (V_{4D-CT}^{Jac}). For SPECT/CT scans, the Q scan (Q_{SPECT}) was acquired first, followed by the V scan (V_{SPECT}). For the 4D-CT ventilation to SPECT comparison, the CT image of SPECT was aligned with the peak-exhale 4D-CT image using rigid image registration. The derived translations and rotations were applied to the SPECT images to align with the 4D-CT ventilation images. The activity-corrected SPECT Q image (Q'_{SPECT}) was subtracted from the V image to determine a net V (V_{SPECT}^{net}).

2.1 Patient

This study was a prospective analysis approved by Stanford University's Institutional Review Board. We studied a radiotherapy patient (66 year-old male) who had a stage IIB lung cancer with a tumor mass in the left upper lobe extending into the left hilum. The patient had a smoking history of 25 pack-years and severe chronic obstructive lung disease (COPD) (GOLD class III).

2.2 4D-CT Pulmonary Ventilation Imaging

4D-CT Scan Acquisition. The 4D-CT ventilation images were created in three steps as follows. The first step was the acquisition of a 4D-CT scan. Four-dimensional CT images are created by acquiring oversampled CT data simultaneously with a respiratory trace and by reconstructing a number of 3D-CT data sets correlated with a given respiratory phase range [14]. The 4D-CT scan was acquired on the GE Discovery ST multislice positron emission CT (PET)/CT scanner (GE Medical Systems, Waukesha, WI) in cine mode with the Varian Real-time Position Management (RPM) system (Varian Medical Systems, Palo Alto, CA) to record patient respiratory traces. The patient was in a supine position. The CT data were acquired at multiple couch positions covering the entire lung for a cine duration that is a little longer than the estimated respiratory period at each position. Audiovisual (AV) biofeedback [15] has been used to improve the patient breathing and to minimize the imaging artifacts. Scan parameters were set as follows: 120 kVp, approximately 100 mAs per slice, 0.5 sec gantry rotation, 0.45 sec cine interval, 512×512 matrix with a pixel size of $1 \text{ mm} \times 1 \text{ mm}$, and 2.5 mm slice thickness, as used clinically in our department. The GE Advantage 4D software was used to create a 4D-CT image set by sorting raw 4D-CT slices correlated with the RPM data into 10 respiratory phase-based bins (i.e., 0% to 90% at 10% intervals). We used paired 4D-CT images at the peak-exhale (60% for the current patient) and peak-inhale (0%) phases for ventilation computation. More details on the 4D-CT acquisition using the GE scanner with Advantage 4D have been described by Rietzel et al. [14]. The 4D-CT scan was acquired before radiotherapy is started.

Deformable Image Registration (DIR). The second step was DIR for spatial voxel-wise mapping of the peak-exhale 4D-CT image to the peak-inhale image, deriving a DVF. To estimate regional ventilation, it is necessary to establish correspondence of the individual respiratory phases. A common method for this task is elastic registration which tries to find a DVF such that one phase image (i.e., peak-inhale 4D-CT image) is transformed into another phase (i.e., peak-exhale). The resulting DVF points from the domain of the peak-exhale image into the domain of the peak-inhale image and therefore can be used for ventilation assessment. Elastic registration minimizes both a certain similarity measure D and a regularizing term S . By adding a regularizing term, the registration problem is well-posed. For D , we chose the sum of squared differences. For S , an elastic regularizer based on the Navier-Lamé equation was employed. The elastic regularizer assumes that the underlying images can be characterized as an elastic and compressible material. Its properties are modeled by the so-called Lamé constants, λ and μ . Based on calculus of variations, we arrive at a system of non-linear partial differential equations to be solved, i.e.,

$$\mu \Delta u + (\mu + \lambda) \nabla \cdot \nabla u = \nabla T_u (R - T_u), \quad (1)$$

where T_u and R correspond to the displaced peak-inhale phase and the peak-exhale phase, respectively. For the discretization of the formula (1), finite differences in conjunction with Neumann boundary conditions have been chosen. The resulting

system of linear equations consists on one hand of a sparse, symmetric and highly structured matrix arising from the regularizer and, on the other hand, of a so-called force vector corresponding to the similarity measure. By nature, the larger the contrast of misaligned image structures is, the larger the modulus of the force vector is. Therefore, bone structures would be perfectly aligned in CT images, whereas soft tissue may not. This holds particularly for the lung-rib interface with on the one side the parenchyma following the motion, and on the other side the ribs staying in place or even moving in opposite direction. To circumvent misalignment of parenchymal structures, we added a simple masking of the force vector. For every voxel with a HU value greater than 0 in the reference phase, the force vector was set to 0 for this voxel location. This results in a lung deformation which is not influenced by misalignment of the rib cage.

Ventilation Computation. The final step was quantitative analysis of the resultant DVFs for computing the ventilation metric. Ventilation can be estimated for each voxel based on the established correspondence between the peak-exhale and peak-inhale 4D-CT images. In this study, we investigated two metrics exploiting: (1) HU-change in corresponding parenchymal structures (V_{4D-CT}^{HU}) [4, 5, 7, 10, 13], or (2) local volume changes of the computed DVF, i.e., Jacobian determinant (V_{4D-CT}^{Jac}) [7, 8, 13]. For V_{4D-CT}^{HU} , we presumed that regional ventilation can be represented by the relative change in fraction of air as originally proposed by Simon [5]. The V_{4D-CT}^{HU} value in the voxel at location (x) of the peak-exhale image is given by,

$$V_{4D-CT}^{HU}(x) = 1000 \frac{HU_{inhale}\{x + u(x)\} - HU_{exhale}(x)}{HU_{exhale}(x)[HU_{inhale}\{x + u(x)\} + 1000]}, \quad (2)$$

where $HU(x)$ is the HU value and $u(x)$ is the displacement vector mapping the voxel at location (x) of the peak-exhale image to the corresponding location of the peak-inhale image. Given the influence of the statistical noise, the CT images have been smoothed with a Gaussian filter kernel with a variance, $\sigma^2 = 1.5 \text{ mm}^2$ before computing V_{4D-CT}^{HU} . For V_{4D-CT}^{Jac} , we presumed that regional ventilation can be represented by a Jacobian determinant of deformation. The V_{4D-CT}^{Jac} value in the voxel at location (x) is given by,

$$V_{4D-CT}^{Jac}(x) = \det[\nabla\{x + u(x)\}] - 1. \quad (3)$$

For both V_{4D-CT}^{HU} and V_{4D-CT}^{Jac} , positive and negative values indicate local expansion and contraction, respectively.

2.3 SPECT/CT V/Q Scan

The SPECT/CT V/Q scan consisted of four parts: (1) CT for SPECT Q (Q_{SPECT}), (2) Q_{SPECT} , (3) CT for SPECT V (V_{SPECT}), and (4) V_{SPECT} . The SPECT/CT V/Q scan was acquired on the GE Infinia Hawkeye SPECT/CT scanner. For Q_{SPECT} , 1 mCi of technetium-99m-labeled macroaggregated albumin ($^{99m}\text{Tc-MAA}$) was injected intravenously. For V_{SPECT} , technetium-99m-labeled diethylenetriamine pentaacetate ($^{99m}\text{Tc-DTPA}$) was aerosolized. The patient's nose was clamped and an inhalation of $^{99m}\text{Tc-DTPA}$ aerosols was given through a mouth piece of a nebulizer until the count

rate reached three times higher than the original count rate recorded after Q_{SPECT} . The SPECT scans were acquired in a 64×64 matrix with a pixel size of $8.8 \text{ mm} \times 8.8 \text{ mm}$ with 60 projections over 360° and durations of 25 s per projection for Q_{SPECT} , and 30 s for V_{SPECT} . The slice thickness was 8.8 mm. The low-dose CT scans were also acquired at 120 kVp and 2.5 mAs. The SPECT images were reconstructed with attenuation correction using the CT images. For the SPECT/CT scan, the patient was in a supine position on a flat Lucite board placed on top of a concave couch in order to reduce registration errors between 4D-CT and SPECT images. Both the SPECT and CT scans were acquired under free breathing as it took long. The SPECT/CT scan was acquired on the same day as 4D-CT and hence the patient was expected to have the same functional status.

2.4 Statistical Analysis

The $V_{4\text{D-CT}}^{\text{HU}}$ and $V_{4\text{D-CT}}^{\text{Jac}}$ images were compared to V_{SPECT} and Q_{SPECT} . Here we assumed V_{SPECT} as ground truth. Q_{SPECT} was also used for the comparison as surrogate of V_{SPECT} , given that there was concern for central airway depositions of aerosol particles in V_{SPECT} for severe COPD patients [16]. The current patient had severe COPD as described above in the section 2.1. Strong correlations between ventilation and perfusion have been demonstrated [17, 18] (e.g., 0.89 [17]), and therefore perfusion can be used as surrogate. For the comparison, the CT image of SPECT was aligned with the peak-exhale 4D-CT image using rigid image registration (Fig. 1). The derived translations and rotations were applied to the SPECT images to align with the 4D-CT ventilation images. Given that V_{SPECT} was acquired after Q_{SPECT} and $^{99\text{m}}\text{Tc-MAA}$ activity remained on V_{SPECT} , the activity-corrected Q_{SPECT} (i.e., Q'_{SPECT}) was subtracted from V_{SPECT} to determine a net V (i.e., $V_{\text{SPECT}}^{\text{net}}$). The activity correction for Q_{SPECT} was simply based on an exponential decrease with a physical half-life of $^{99\text{m}}\text{Tc}$ (i.e., 6 h) and a biological half-life of MAA (i.e., 5 h [19]). After registration, the Spearman's rank correlation coefficients were determined to quantify the correlation between $V_{4\text{D-CT}}^{\text{HU}}$ or $V_{4\text{D-CT}}^{\text{Jac}}$ and $V_{\text{SPECT}}^{\text{net}}$ or Q_{SPECT} . For the correlation analysis, the 4D-CT ventilation images were downsampled to the SPECT image resolution.

3 Results

Fig. 2 shows example images of 4D-CT, $V_{4\text{D-CT}}^{\text{HU}}$, $V_{4\text{D-CT}}^{\text{Jac}}$, $V_{\text{SPECT}}^{\text{net}}$ and Q_{SPECT} . The V and Q images are shown with a scale from the 10th percentile value to the 90th percentile value. The percentile values were determined for the V or Q values inside the lungs. The $V_{4\text{D-CT}}$ images provided a higher resolution than $V_{\text{SPECT}}^{\text{net}}$ or Q_{SPECT} . In the comparison between $V_{4\text{D-CT}}^{\text{HU}}$ or $V_{4\text{D-CT}}^{\text{Jac}}$ and $V_{\text{SPECT}}^{\text{net}}$, there were several agreements in some regions and many disagreements throughout the lungs. Overall, all V images showed higher ventilation in the right lung than in the left lung, which would be due to a large tumor mass near the left hilum compressing large bronchi. For $V_{4\text{D-CT}}^{\text{HU}}$, we found reasonable agreements in the right lower region at mid-anterior (low ventilation) and in the right upper region at mid-posterior and posterior

(high ventilation) for example. However, disagreements were more obvious and were found throughout the lungs, e.g., V_{4D-CT}^{HU} showed moderate ventilation in the left lung at anterior and mid-anterior, where V_{SPECT}^{net} showed high ventilation. In addition, we found disagreements in periphery, where V_{4D-CT}^{HU} showed higher ventilation than V_{SPECT}^{net} . Presumably these disagreements are due to central airway depositions of aerosol particles in V_{SPECT}^{net} as observed at mid-posterior, which would underrepresent peripheral ventilation. The Spearman voxel-based correlation coefficient between V_{4D-CT}^{HU} and V_{SPECT}^{net} was 0.030. Similarly V_{4D-CT}^{Jac} also had many disagreements with V_{SPECT}^{net} and the correlation was 0.184. Fig. 3 shows the voxel-based relationships between V_{4D-CT}^{HU} or V_{4D-CT}^{Jac} and V_{SPECT}^{net} or Q_{SPECT} . There were considerable probabilities of negative 4D-CT ventilation values that are not supposed to appear during inhalation in principle, as observed by Christensen et al. [9]. This leaves open the question of DIR algorithm errors.

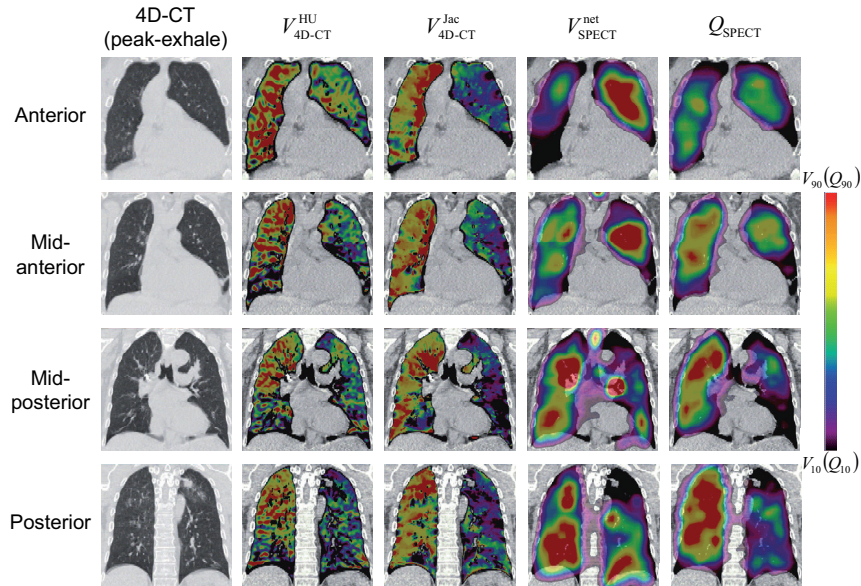


Fig. 2. Example images at the same coronal level of peak-exhale 4D-CT, 4D-CT ventilation derived by the Hounsfield unit (HU) metric (V_{4D-CT}^{HU}) or the Jacobian metric (V_{4D-CT}^{Jac}), the net SPECT ventilation (V_{SPECT}^{net}), and perfusion (Q_{SPECT}). Each row represents different coronal level. The ventilation and perfusion images are shown with a scale from the 10th percentile value (V_{10} or Q_{10}) to the 90th percentile value (V_{90} or Q_{90}). The x th percentile value is the ventilation (perfusion) value at which $x\%$ of the total lung volume has lower value. Note that the V_{4D-CT} values outside the lungs are masked out, while V_{SPECT}^{net} and Q_{SPECT} are not masked out to show central airway depositions of aerosol particles in the V_{SPECT}^{net} image.

In the comparison between V_{4D-CT}^{HU} or V_{4D-CT}^{Jac} and Q_{SPECT} , there were both agreements and disagreements as with V_{SPECT}^{net} , however there were clearly more agreements for Q_{SPECT} compared to V_{SPECT}^{net} from visual inspection (Fig. 2). The Q_{SPECT}

image also showed higher perfusion in the right lung than in the left lung similarly to the V images, which would be due to a large tumor compressing large vessels. For V_{4D-CT}^{HU} , we found reasonable agreements in the left upper region at anterior and mid-anterior (moderate ventilation) and in the right upper region at mid-posterior (high ventilation) for example. Disagreements were found in the right lung at anterior for example, where V_{4D-CT}^{HU} showed high ventilation, however Q_{SPECT} showed low to moderate ventilation. The Spearman voxel-based correlation coefficient between V_{4D-CT}^{HU} and Q_{SPECT} was 0.357 (Fig. 3). V_{4D-CT}^{Jac} also demonstrated better agreements with Q_{SPECT} than with V_{SPECT}^{net} and the correlation coefficient was 0.479.

Two different ventilation metrics led to spatially variant 4D-CT ventilation images (V_{4D-CT}^{HU} and V_{4D-CT}^{Jac}) (Fig. 2). From visual inspection, there were good agreements in the right upper region at mid-posterior (high ventilation) and in the left lung at posterior (low ventilation). However, V_{4D-CT}^{HU} showed low ventilation in the right lower region at mid-anterior and mid-posterior, where V_{4D-CT}^{Jac} showed high ventilation in contrast. The Spearman voxel-based correlation coefficient between V_{4D-CT}^{HU} and V_{4D-CT}^{Jac} was 0.459. Also, V_{4D-CT}^{HU} demonstrated a more heterogeneous distribution with a coefficient of variation (i.e., the ratio of the standard deviation to the mean) of 0.160 than V_{4D-CT}^{Jac} with 0.072, which is reflected in more scattered distributions in Fig. 3.

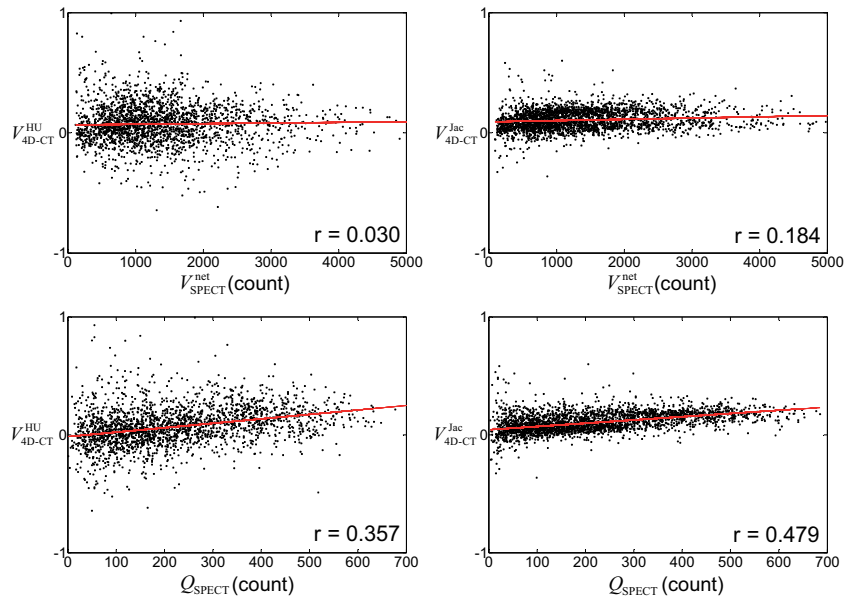


Fig. 3. Four-dimensional (4D) computed tomography (CT) ventilation vs. single photon emission CT (SPECT) ventilation or perfusion. The Spearman correlation coefficients and least square regression lines are also shown.

4 Discussion

The correlations between the 4D-CT ventilation and SPECT ventilation (assumed ground truth) were weak, which is consistent with Castillo et al. [6]. The weak correlations could be due to limitations of the 4D-CT and/or SPECT techniques. The limitations of the 4D-CT ventilation imaging technique include (1) a potential bias in the HU metric, (2) the need for the physiologic validation, and (3) the artifacts in 4D-CT images. There is a possibility that the HU metric underestimates the actual HU change, given that the DIR algorithm used in this study minimizes the sum of squared differences, however this effect would be small considering that it is also based on the elastic regularizer. Our recent study demonstrated significantly lower ventilation in emphysematous lung regions than in non-emphysematous regions ($p < 0.001$), which indicates a potential of 4D-CT ventilation imaging to achieve the high physiologic accuracy [13]. However, this study focused on the global accuracy only. Artifacts are observed in the 4D-CT images at an alarmingly high frequency (i.e., 90%) [20], which could impact 4D-CT ventilation imaging. Although we used AV biofeedback to minimize the artifacts, several artifacts still remained in the images. There are several more strategies to improve 4D-CT, including a wide-area detector CT scanner with a greater coverage [21], improved sorting methods [22, 23], and post-scan image processing [24, 25]. The limitations of the SPECT ventilation scan with ^{99m}Tc -DTPA aerosols include central airway depositions in severe COPD patients [16]. That was the case in the current study as the patient had severe COPD. Central deposition limits the uniform penetration of aerosol particles to periphery, yielding non-representative SPECT ventilation [26, 27]. In a recent study, an ultrafine dispersion of technetium-99m-labeled carbon (i.e., Technegas) has been found to be superior to ^{99m}Tc -DTPA for COPD patients [26]. In addition to these limitations of the 4D-CT and SPECT techniques, several differences between these two techniques might lead to the weak correlation. The differences include the spatial resolution, patient positioning and respiratory phase. For the difference in the resolution, appropriate smoothing for creating a 4D-CT ventilation image may result in an improved correlation. The patient received the 4D-CT and SPECT scans separately on the different scanners, where there was a considerable difference in positioning even though we tried to minimize it. We would not be able to disregard this difference unless a SPECT/CT scanner with the 4D-CT capability is used to acquire both 4D-CT and SPECT scans. The difference in the respiratory phase is another issue, i.e., the 4D-CT ventilation was based on the peak-exhale and peak-inhale phases only, however the SPECT ventilation was acquired under free breathing. Integrating the 4D-CT ventilation created from all the 4D-CT images over a full respiratory cycle would more appropriately represent free breathing and may improve a correlation.

The correlations between the 4D-CT ventilation and SPECT perfusion were much higher than those with the SPECT ventilation. However, they were still weak, which could be due to a potential difference between ventilation and perfusion in addition to limitations of the 4D-CT and/or SPECT techniques as described above. It has been demonstrated that regional ventilation is tightly matched to perfusion in large laboratory animals under normal conditions [17, 18], even though its mechanisms

remain unresolved. Altemeier found a strong correlation between ventilation and perfusion in pigs with an average correlation coefficient of 0.89 [17]. There are several potential causes degrading this matching, which include pathological conditions and mechanical ventilation [28]. Mismatch between ventilation and perfusion occurs mainly due to pulmonary vascular disease such as pulmonary embolism and hypoplasia/aplasia of pulmonary artery [19]. In this study, the patient had no clear evidence of such diseases, however had a lung cancer and COPD that might degrade the ventilation and perfusion matching. Another difference may come from the effect of posture and gravity on the relationship between ventilation and perfusion [29, 30]. Recently, Petersson et al. investigated this effect using the SPECT V/Q scan for 7 healthy volunteers in a supine posture [29]. They found more uniform V/Q ratios close to 1 in the superior-inferior direction compared to an upright posture, however there were slight increases up to approximately 1.3 in the inferior regions.

The 4D-CT ventilation imaging technique has higher spatial and temporal resolution, lower cost, shorter scan time, and/or higher accessibility compared with other techniques (including nuclear medicine, hyperpolarized gas MR, and Xe-CT). The 4D-CT ventilation can be considered as 'free' information, because 4D-CT scans are in routine use for lung cancer radiotherapy in many centers, and ventilation computation involves only image processing (DIR) and analysis. Furthermore, 4D-CT ventilation imaging has an inherent advantage, i.e., perfect registration to the original CT images, which enables high-resolution anatomic correlation. Once validated, 4D-CT ventilation images could be used in lung cancer radiotherapy to avoid high-functional lung regions from radiation that may allow pulmonary toxicity reduction [31, 32]. Also, the functional response to radiotherapy treatment could be investigated with 4D-CT ventilation imaging.

5 Conclusion

The physiologic accuracy of 4D-CT ventilation imaging has been quantitatively evaluated on a human subject by comparison with the SPECT/CT V/Q scan. The correlation between the 4D-CT ventilation and SPECT V was very weak, where the SPECT V showed significant central airway depositions of aerosol particles. The correlation between the 4D-CT ventilation and SPECT Q was much higher, which indicates a potential of 4D-CT ventilation imaging to achieve the high physiologic accuracy. A further study is necessary to investigate the differences between the 4D-CT ventilation and SPECT V/Q and to improve the accuracy through acquiring more patient data including non-COPD patients.

Acknowledgments. Julian Hong, Lindee Burton, and Jayesh Patel at Stanford University provided significant assistance with the patient accrual process and the study coordination. Dr. Guoqiang Cui at Stanford assisted with AV biofeedback for the 4D-CT scan.

References

1. Suga, K.: Technical and analytical advances in pulmonary ventilation SPECT with xenon-133 gas and Tc-99m-Technegas. *Ann Nucl Med* **16** (2002) 303-310
2. Fain, S.B., Korosec, F.R., Holmes, J.H., O'Halloran, R., Sorkness, R.L., Grist, T.M.: Functional lung imaging using hyperpolarized gas MRI. *J Magn Reson Imaging* **25** (2007) 910-923
3. Simon, B.A.: Regional ventilation and lung mechanics using X-Ray CT. *Acad Radiol* **12** (2005) 1414-1422
4. Guerrero, T., Sanders, K., Noyola-Martinez, J., Castillo, E., Zhang, Y., Tapia, R., Guerra, R., Borghero, Y., Komaki, R.: Quantification of regional ventilation from treatment planning CT. *Int J Radiat Oncol Biol Phys* **62** (2005) 630-634
5. Simon, B.A.: Non-invasive imaging of regional lung function using x-ray computed tomography. *J Clin Monit Comput* **16** (2000) 433-442
6. Castillo, R., Castillo, E., Martinez, J., Guerrero, T.: Ventilation from four-dimensional computed tomography: density versus Jacobian methods. *Phys Med Biol* **55** (2010) 4661-4685
7. Kabus, S., von Berg, J., Yamamoto, T., Opfer, R., Keall, P.J.: Lung ventilation estimation based on 4D-CT imaging. *Proc. of the First International Workshop on Pulmonary Image Analysis, MICCAI 2008* (2008) 73-81
8. Reinhardt, J.M., Ding, K., Cao, K., Christensen, G.E., Hoffman, E.A., Bodas, S.V.: Registration-based estimates of local lung tissue expansion compared to xenon CT measures of specific ventilation. *Med Image Anal* **12** (2008) 752-763
9. Christensen, G.E., Song, J.H., Lu, W., El Naqa, I., Low, D.A.: Tracking lung tissue motion and expansion/compression with inverse consistent image registration and spirometry. *Med Phys* **34** (2007) 2155-2163
10. Guerrero, T., Sanders, K., Castillo, E., Zhang, Y., Bidaut, L., Pan, T., Komaki, R.: Dynamic ventilation imaging from four-dimensional computed tomography. *Phys Med Biol* **51** (2006) 777-791
11. Brock, K.K.: Results of a Multi-Institution Deformable Registration Accuracy Study (MIDRAS). *Int J Radiat Oncol Biol Phys* **76** (2009) 583-596
12. Kashani, R., Hub, M., Balter, J.M., Kessler, M.L., Dong, L., Zhang, L., Xing, L., Xie, Y., Hawkes, D., Schnabel, J.A., McClelland, J., Joshi, S., Chen, Q., Lu, W.: Objective assessment of deformable image registration in radiotherapy: a multi-institution study. *Med Phys* **35** (2008) 5944-5953
13. Yamamoto, T., Kabus, S., von Berg, J., Klinder, T., Blaffert, T., Lorenz, C., Keall, P.J.: Physiological validation of 4D-CT-based ventilation imaging in patients with chronic obstructive pulmonary disease (COPD). *Med Phys* **36** (2009) 2821 (Abstract)
14. Rietzel, E., Pan, T., Chen, G.T.: Four-dimensional computed tomography: image formation and clinical protocol. *Med Phys* **32** (2005) 874-889
15. Venkat, R.B., Sawant, A., Suh, Y., George, R., Keall, P.J.: Development and preliminary evaluation of a prototype audiovisual biofeedback device incorporating a patient-specific guiding waveform. *Phys Med Biol* **53** (2008) N197-N208
16. Magnant, J., Vecellio, L., de Monte, M., Grimbert, D., Valat, C., Boissinot, E., Guilloateau, D., Lemarie, E., Diot, P.: Comparative analysis of different scintigraphic approaches to assess pulmonary ventilation. *J Aerosol Med* **19** (2006) 148-159

17. Altemeier, W.A., Robertson, H.T., Glenny, R.W.: Pulmonary gas-exchange analysis by using simultaneous deposition of aerosolized and injected microspheres. *J Appl Physiol* **85** (1998) 2344-2351
18. Melsom, M.N., Kramer-Johansen, J., Flatebo, T., Muller, C., Nicolaysen, G.: Distribution of pulmonary ventilation and perfusion measured simultaneously in awake goats. *Acta Physiol Scand* **159** (1997) 199-208
19. Ziessman, H.A., O'Malley, J.P., Thrall, J.H.: *Nuclear Medicine: The Requisites*. A Mosby Title (2005)
20. Yamamoto, T., Langner, U., Loo, B.W., Jr., Shen, J., Keall, P.J.: Retrospective analysis of artifacts in four-dimensional CT images of 50 abdominal and thoracic radiotherapy patients. *Int J Radiat Oncol Biol Phys* **72** (2008) 1250-1258
21. Mori, S., Endo, M., Tsunoo, T., Kandatsu, S., Tanada, S., Aradate, H., Saito, Y., Miyazaki, H., Satoh, K., Matsushita, S., Kusakabe, M.: Physical performance evaluation of a 256-slice CT-scanner for four-dimensional imaging. *Med Phys* **31** (2004) 1348-1356
22. Rietzel, E., Chen, G.T.: Improving retrospective sorting of 4D computed tomography data. *Med Phys* **33** (2006) 377-379
23. Lu, W., Parikh, P.J., Hubenschmidt, J.P., Bradley, J.D., Low, D.A.: A comparison between amplitude sorting and phase-angle sorting using external respiratory measurement for 4D CT. *Med Phys* **33** (2006) 2964-2974
24. Ehrhardt, J., Werner, R., Saring, D., Frenzel, T., Lu, W., Low, D., Handels, H.: An optical flow based method for improved reconstruction of 4D CT data sets acquired during free breathing. *Med Phys* **34** (2007) 711-721
25. Schreiber, E., Chen, G.T., Xing, L.: Image interpolation in 4D CT using a BSpline deformable registration model. *Int J Radiat Oncol Biol Phys* **64** (2006) 1537-1550
26. Jogi, J., Jonson, B., Ekberg, M., Bajc, M.: Ventilation-perfusion SPECT with ^{99m}Tc-DTPA versus Technegas: a head-to-head study in obstructive and nonobstructive disease. *J Nucl Med* **51** (2010) 735-741
27. Agnew, J.E., Francis, R.A., Pavia, D., Clarke, S.W.: Quantitative comparison of ^{99m}Tc-aerosol and ⁸¹Kr ventilation images. *Clin Phys Physiol Meas* **3** (1982) 21-30
28. Glenny, R.W.: Determinants of regional ventilation and blood flow in the lung. *Intensive Care Med* **35** (2009) 1833-1842
29. Petersson, J., Rohdin, M., Sanchez-Crespo, A., Nyren, S., Jacobsson, H., Larsson, S.A., Lindahl, S.G., Linnarsson, D., Neradilek, B., Polissar, N.L., Glenny, R.W., Mure, M.: Regional lung blood flow and ventilation in upright humans studied with quantitative SPECT. *Respir Physiol Neurobiol* **166** (2009) 54-60
30. Musch, G., Layfield, J.D., Harris, R.S., Melo, M.F., Winkler, T., Callahan, R.J., Fischman, A.J., Venegas, J.G.: Topographical distribution of pulmonary perfusion and ventilation, assessed by PET in supine and prone humans. *J Appl Physiol* **93** (2002) 1841-1851
31. Yamamoto, T., Kabus, S., von Berg, J., Lorenz, C., Keall, P.J.: Impact of four-dimensional computed tomography pulmonary ventilation imaging-based functional avoidance for lung cancer radiotherapy. *Int J Radiat Oncol Biol Phys* **In press** (2010)
32. Yaremko, B.P., Guerrero, T.M., Noyola-Martinez, J., Guerra, R., Lege, D.G., Nguyen, L.T., Balter, P.A., Cox, J.D., Komaki, R.: Reduction of normal lung irradiation in locally advanced non-small-cell lung cancer patients, using ventilation images for functional avoidance. *Int J Radiat Oncol Biol Phys* **68** (2007) 562-571